J Mater Sci (2009) 44:6490–6497
DOI 10.1007/s10853-009-3321-2

MESOSTRUCTURED MATERIALS

Three-dimensional titania pore structures produced by using a femtosecond laser pulse technique and a dip coating procedure

Falk Heinroth · Simon Münzer · Armin Feldhoff · Sven Passinger · Wei Cheng · Carsten Reinhardt · Boris Chichkov · Peter Behrens

Received: 30 November 2008 / Accepted: 4 February 2009 / Published online: 9 March 2009

Abstract In this work, the preparation of three-dimensional hierarchical pore structures by a combination of laser-based templates and the self-organization process of mesostructured titania is presented. For this purpose macrostructured polymers produced by two-photon polymerization act as a template for the deposition of a mesostructured titania film from a solution containing an amphiphilic block copolymer by dip coating. A carefully applied calcination procedure removes both the macrotemplating polymer and the mesotemplating surfactant molecules so that a replica of the initial polymer structure with a hierarchical (macro- and meso-) pore system is obtained. In addition, the titania, which is amorphous after deposition, is transferred into crystalline anatase during calcination. Materials with dual pore systems are interesting for possible applications in catalysis and sorption, and three-dimensional crystalline structures from materials with high refraction index are attractive for photonic applications, for example as photonic crystals.

F. Heinroth · S. Münzer · P. Behrens (✉)
Institut für Anorganische Chemie, Leibniz Universität Hannover, Callinstraße 9, Hannover 30167, Germany
e-mail: peter.behrens@acb.uni-hannover.de

A. Feldhoff
Institut für Physikalische Chemie und Elektrochemie, Leibniz Universität Hannover, Callinstraße 3A, Hannover 30167, Germany

S. Passinger · W. Cheng · C. Reinhardt · B. Chichkov
Laser Zentrum Hannover e.V., Hollerithallee 8, Hannover 30419, Germany

Introduction

Current investigations in femtosecond laser technology have developed a new field of synthesis strategies for the creation of three-dimensional structures. With this approach, structures in micro- and nanometer dimensions are available. The obtained 3D structures are interesting for micromechanical [1] and microoptical [2–8] devices as well as for biomedical and biotechnical applications [1, 9]. For the fabrication of these structures a non-linear polymerization process is used. By this procedure a photosensitive polymeric resin is polymerized by two-photon absorption of near-infrared femtosecond laser pulses from a Ti: sapphire-based laser system. The two-photon-polymerization (2PP) is accomplished by an operating wavelength of around 800 nm. Only when the femtosecond laser pulses are tightly focused inside the volume of a photosensitive resin, a polymerization reaction is initiated. In contrast to polymerization reactions initiated with UV light, IR-based 2PP allows direct writing within the volume of the polymeric resin [5, 10]. Hence, the fabrication of any imaginable computer-generated 3D structure can be carried out. So far resolutions of 3D structures down to 100 nm were attained by using the 2PP technique.

Due to their special pore properties and resulting large surface areas, ordered mesoporous materials have been in the focus of scientific interest for many years since the first examples were presented by Mobil Oil Co. in 1992 [11, 12]. They form by a self-organized process from solutions of inorganic precursor species and amphiphiles and are attractive for application in sorption and separation processes [13] as well as in catalysis [14]. In addition to the well-known mesoporous silica materials, also other interesting materials, for instance transition metal oxides [15], sulfides [16], phosphates [17], and borates [18] have been used for the preparation of ordered mesoporous systems.

Other investigations have been carried out to obtain special morphologies in addition to the powder substances obtained in standard syntheses. Highly ordered mesoporous thin films have for example been obtained for silica and titania [19, 20] by the evaporation-induced self-assembly process (EISA) [21, 22]. Thin films with an ordered pore system are interesting for applications as sensors [23] and as biomaterials, for example in tissue engineering, drug delivery, and medical implants [24].

Recently, we have shown that these two approaches, the "top down" approach represented by the 2PP technique and the chemical self-assembly "bottom up" synthesis of a mesostructured material, can be combined. In this case, we have used silica precursors and have produced macro-/mesoporous materials [25]. Such hierarchically structured dual pore system materials could have interesting applications in biomedicine and in catalysis. However, for applications in photonics and optic devices, the refraction index of silica is too low. The distinguished property of a photonic crystal is a full 3D band gap, preferably in the visible range. The challenge in the fabrication of photonic crystals lies in creating a pre-defined 3D structure with high perfection which consists of a material with a high refraction index. With the 2PP technique, a method to produce high-quality 3D structures is established but unfortunately the refraction index of the used polymeric resins is also too low for suitable applications in photonics. However, the polymer structure could be used as a template for the creation of a 3D structure from a material with higher refraction. So far, different methods like chemical vapor deposition (CVD) and atomic layer deposition (ALD) as well as different materials like silicon and germanium were used with this purpose. However, these procedures included inconvenient preparations steps, for example a washing procedure with hydrofluoric acid [26, 27].

In this work, we present the preparation of a three-dimensional hierarchical titania structure which is macro- and mesoporous. A scheme of the synthesis strategy is illustrated in Fig. 1. A three-dimensional polymer structure produced by the 2PP technique is used as a template for the deposition of a titania mesostructure, which is formed due to the templating action of a surfactant [28–30]. By a special calcination procedure the macrostructured polymers as well as the mesotemplating surfactant molecules are removed and a three-dimensional hierarchical pore structure of titania is obtained. The formation of non-porous silica–titania-based replicas via a similar approach has recently been described [31].

Experimental

Template fabrication by two-photon polymerization

For the fabrication of high-resolution macrostructures an immersion oil APOPLAN microscope objective from Zeiss (Germany) with a numerical aperture of 1.4 and a magnification of 100 was used. In the experiments, a Yb–glass femtosecond oscillator from Polar Lasers (Hannover, Germany) with subsequent frequency doubling was applied. This system delivered laser pulses at 1030 nm (515 nm after frequency doubling) with a duration of 200 fs

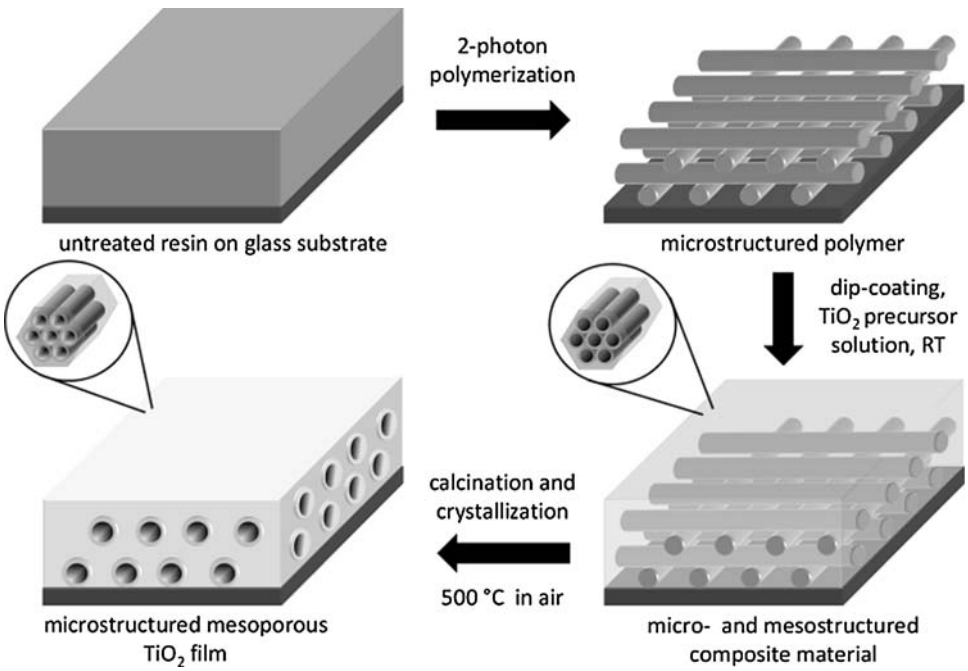

Fig. 1 Synthetic strategy for the combination of 2-photon polymerization and the self-organization process of mesostructured titania

(FWHM) and a repetition rate of 1 MHz. Average powers around 2 mW at 515 nm and writing speeds of several mm/s were applied for the structuring of the used polymer. As a setup for structuring, the commercial Micro-3-Dimensional Structuring System (M3D) from the Laser Zentrum Hannover e. V. (Hannover, Germany) was used. The principal design of this setup reported elsewhere [32] consisted of the 80 MHz acousto-optic modulator from Landwehr (Norderstedt, Germany) as fast shutter system, a $\lambda/2$-waveplate in combination with a polarizing beamsplitter for energy adjustment, and a telescope as beam expanding optics. The laser processing was imaged by a CCD camera viewing along the laser beampath through a dichroic mirror. The structuring was accomplished by using a high-precession XYZ positioning system consisting of three ABL1000-axes from Aerotech GmbH (Nürnberg, Germany) with an overall travel range of $15 \times 10 \times 10$ cm^3.

The lines and woodpile structures used in these investigations have been fabricated in the epoxy resin SU8 from Gersteltec (Switzerland). The material was spin coated on a microscopy glass slide of 18×18 mm^2 area and 170 μm thickness. This glass slide was fixed bottom upwards in the sample holder below the microscope objective allowing an illumination of the polymer through the glass slide. After the polymerization step, the non-irradiated material was removed by using 1-methoxy-2-propyl acetate as solvent.

Mesostructured titania

Mesostructured amorphous titania films and resultant crystalline titania films were prepared with the following procedure [29]. $EO_{106}PO_{70}EO_{106}$ of 1.7 g ($M_{av} = 13300$ g mol^{-1}, Aldrich) was dissolved in 45 mL ethanol. To this solution 2.85 mL $TiCl_4$ and 1.87 mL H_2O were carefully added dropwise. In a second solution 2.81 mL H_2O and 1.4 mL nitromethane were mixed and slowly added to the first solution. The combined solution was stirred for 30 min at 80 °C and subsequently the ethanol was removed from the solution so that a viscous gel was obtained. Glass substrates with microstructured polymer films were then dipped immediately into the solution with a NIMA DC Mono 75 dip-coater. The immersion speed was set to 10 mm min^{-1} and the holding time on the lowest point (inside the liquid) was 10 s. The obtained films were dried for 30 min above the reaction solution and for 3 days in a desiccator above a saturated $Mg(NO_3)_2$ solution, regulating humidity to approximately 50–60%. To reduce crack formation due to the shrinkage of the titania films, the samples were post-treated for 24 h at 60, 80, and 130 °C, respectively. Crystallization of the amorphous titania film and calcination of the polymer were carried out at 500 °C in air for 1 h with a temperature ramp of 1 °C min^{-1}.

Characterization

Small-angle X-ray scattering (SAXS) data were recorded on a system from Rigaku (Japan) with a Bede microfocus X-ray source, an Osmic MaxFlux confocal X-ray optic (CuK_α radiation, $\lambda = 1.541$ Å), a three-pinhole collimation, and a gas-filled 2D multiwire detector. The detector was calibrated using a silver behenate powder standard. The samples were observed within secondary electron (SE) contrast using a JSM-6700F cold field-emission gun scanning electron microscope (CFEG-SEM) by JEOL Ltd. (Tokyo, Japan). All samples were coated with a thin layer of gold before the measurements were performed at an accelerating voltage of 2.0 kV and at a working distance of 8 mm. Scanning transmission electron microscopy (STEM) was conducted at 200 kV in high-angle annular dark-field (HAADF) contrast on a field-emission instrument of the type JEM-2100F by JEOL Ltd. The specimen for STEM investigation was prepared by epoxy gluing a sandwich with a mirror-smooth silicon crystal. By cutting and subsequent grinding and polishing a cross section of ca. 10 μm in thickness was observed, which was epoxy glued onto a copper slot grid and finally thinned by argon ion bombardment to local electron transparency.

Results and discussion

For the creation of a three-dimensional titania structure, a polymeric woodpile structure produced with the 2PP technique was used. The polymeric woodpile structure shown in Fig. 2a had a length of 400×400 μm and consisted of four layers (this small number of layers allows better observation of the covered structure in SEM). The rods of the used woodpile structure shown in Fig. 2b had a width of 0.5 μm and a period of 3 μm. Due to the dimension of the rods the resulting pore size of the woodpile structure is 3×3 μm. SEM images of a woodpile structure treated with the dip-coating method described above are given in Fig. 3. In overview (Fig. 3a) the entire structure is illustrated after the dip-coating procedure. In SEM images at higher magnification (Fig. 3b) it becomes obvious that the titania is deposited as a thick film on the entire glass substrate as well as on the woodpile structure. As a consequence three-quarters of the woodpile structure are filled with titania (Fig. 3c and d). Despite the careful drying procedure, crack formation can be observed next to the coated woodpile structure on the glass substrate (Fig. 3a and b). It is interesting to point out that the wide cracks do not exist in the woodpile structure. Only in SEM images taken at higher magnification (Fig. 3c and d), many fine cracks on the interface between the titania and the polymer can be detected. Probably due to these small

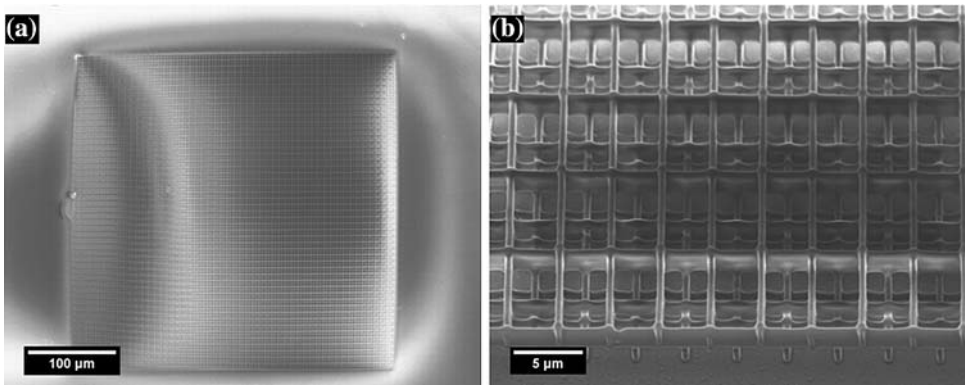

Fig. 2 SEM images of untreated woodpile structure at different magnifications

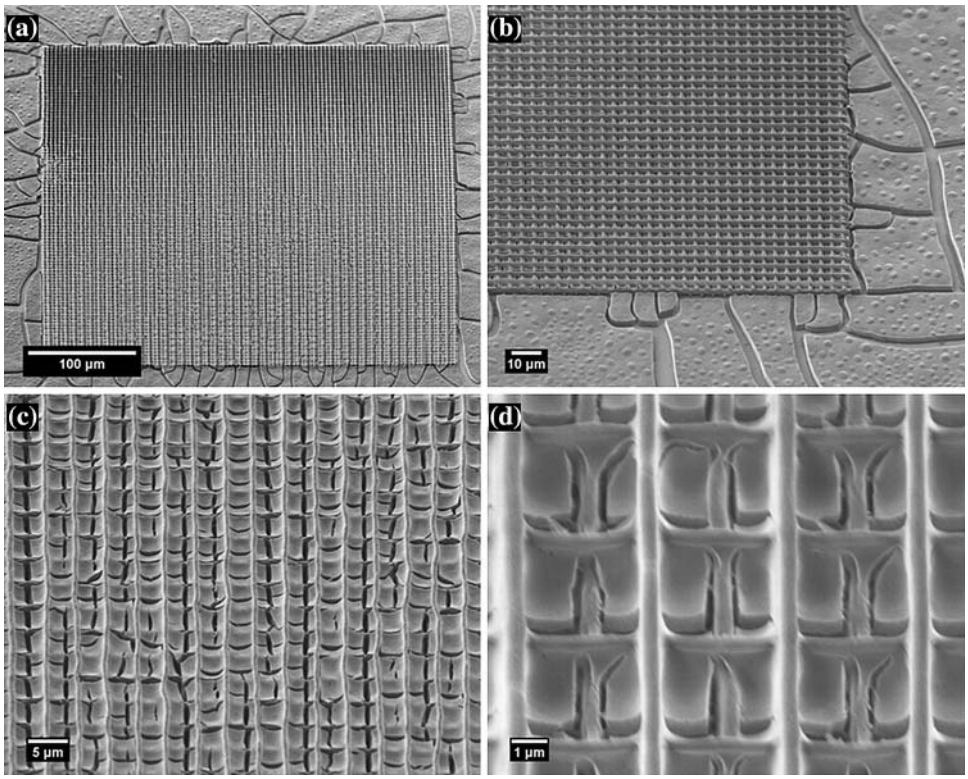

Fig. 3 SEM images at different magnifications of a woodpile structure covered with as-synthesized mesostructured titania

fissures the formation of wide cracks in the woodpile structure is inhibited. The reason of crack formation is the volume shrinkage during drying of amorphous titania, which is well documented in the literature [28].

For the creation of a continuous titania film, in addition to simple drying a controlled post-treatment is necessary to increase condensation and consequently the formation of a stable network. Hence the temperature for the post-synthetic treatment was increased in small steps from 60 °C to 80 °C and finally to 130 °C; each treatment lasted for 24 h. SEM images of a coated woodpile structure after the post-treatment are shown in Fig. 4. The overview images (Fig. 4a and b) reveal that the cracks in the titania layer on the surface of the glass substrate have not grown significantly during the treatment. SEM images of the coated woodpile structure at higher magnification (Fig. 4c and d) look very similar to the images before the post-treatment.

After calcination at 500 °C the polymer resin of the woodpile structure as well as the block-copolymer responsible for the mesostructuring of titania were burnt off and formed volatile products. At this high temperature and with the heating ramp used, in addition amorphous titania is transformed into a crystalline product. Figure 5 shows SEM images of such a calcined sample after calcination. In SEM images taken at lower magnification, it is obvious that the titania film on the glass substrate has shrunk drastically (Fig. 5a and b). Interestingly, the replicated woodpile structure is affected considerably less strongly by the volume shrinkage of the titania film. SEM images taken at higher magnification (Fig. 5c and d) reveal a kind of

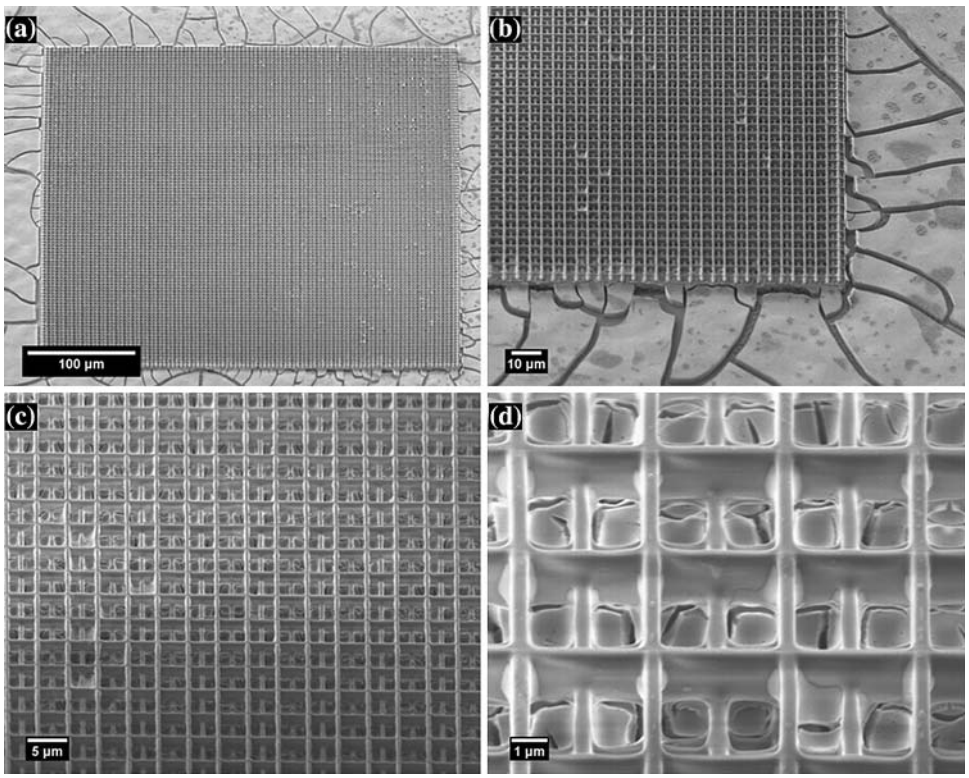

Fig. 4 SEM images at different magnifications of a woodpile structure covered with mesostructured titania after the post-synthetic treatment

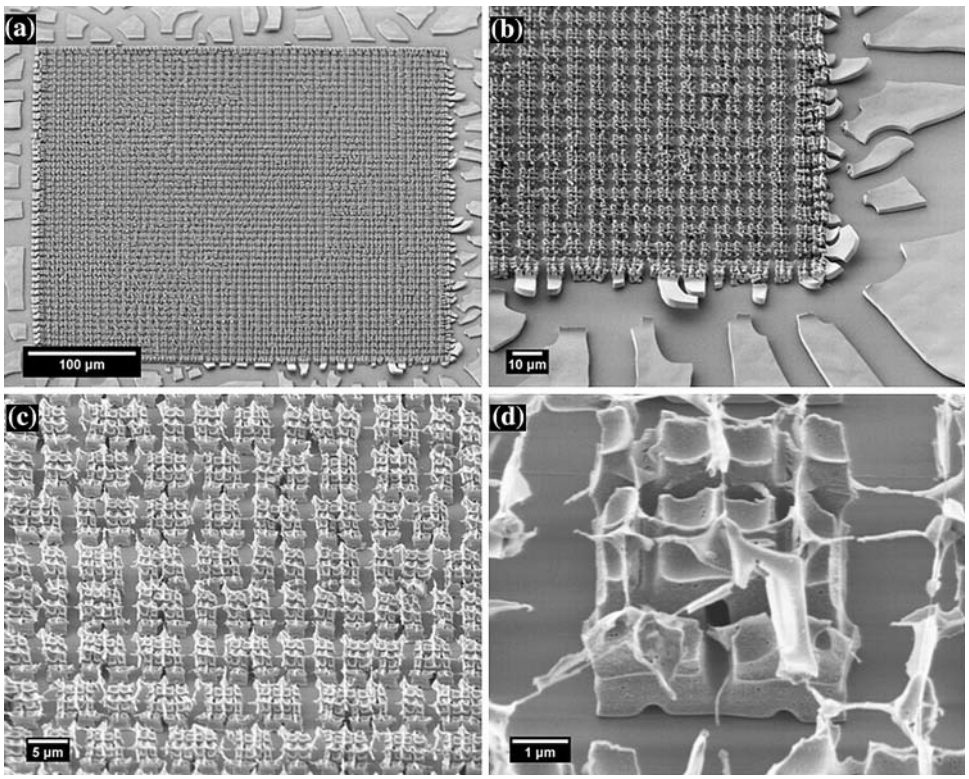

Fig. 5 SEM images at different magnifications of an inverse woodpile structure of titania after calcination

spatial organization of the formed cracks, as apparent from the nearly periodic patterning observed in Fig. 5c. The entire structure consists of regularly spaced square blocks with a width of 5 × 5 µm. Possibly, the small fissures on the interface between polymer and titania described above act as predetermined breaking points; thus, the structure does not shrink in an uncontrolled fashion as the titania on the glass substrate. One of these blocks is displayed in

Fig. 5d. The bottom part of the woodpile structure which was completely filled with titania has formed an inverse replica of the polymeric template structure. The former rods appear as tubes in the remaining blocks. The top quarter of the polymer structure which was only coated by a thin titania film consists of a fragile residue of a shell structure after calcination. Evidently the fine structure connects the titania blocks of the inverse replica. Nevertheless, it is an important result that crack formation caused by the volume shrinkage of titania upon calcination could be in part controlled by the underlying polymer structure.

To prove the existence of a mesostructure in the initially deposited titania film, small-angle X-ray scattering (SAXS) data were collected. The obtained SAXS patterns are shown in Fig. 6. Reflections in the as-synthesized sample after drying (Fig. 6a) can be indexed as (110) and (200) for a body centered cubic mesostructure ($Im\bar{3}m$). Due to absence of the (210) reflection a lowly ordered mesostructure can be assumed. On basis of the observed reflections, a lattice constant of 169 Å is calculated. These results are comparable to those published by Grosso et al. for titania films prepared by the EISA approach [29], although the lattice constant obtained here is 6% smaller. After post-synthetic treatment, the (210) reflection can be observed in addition (Fig. 6b). The appearance of this reflection is an indication of a well-ordered mesostructure after heat treatment. A lattice constant of 154 Å is calculated. The difference between the lattice constants may be explained by a progressive condensation of titania and has also been described in the literature [28]. In the SAXS pattern of the calcined sample (Fig. 6c), no small-angle reflections can be observed anymore, corresponding to a loss of the ordered mesostructure. This phenomenon is also well known in the literature [29, 30].

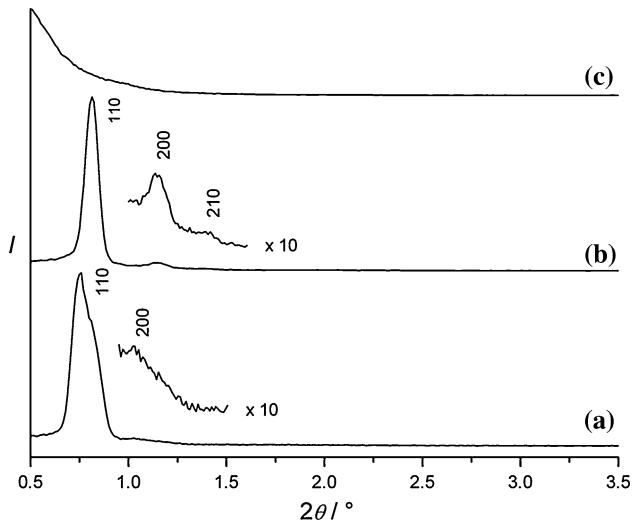

Fig. 6 SAXS pattern of a woodpile structure after (a) coating with as-synthesized mesostructured titania, (b) post-synthetic treatment, (c) calcination

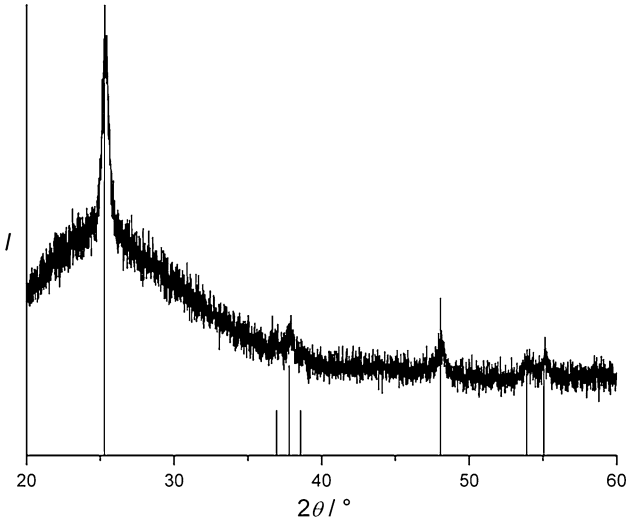

Fig. 7 XRD pattern of an inverted woodpile of titania after calcination (reference lines: anatase [33])

The reason for this loss of order can be found in the phase transition of amorphous titania to crystalline anatase, as evidenced by the powder X-ray diffraction pattern depicted in Fig. 7. To test whether during this transformation the mesoporosity of the sample is totally lost, we carried out advanced transmission electron microscopy investigations. For this purpose a cross-sectional STEM analysis was performed (Fig. 8). The cross-sectional area shown in Fig. 8a confirms the observation from SEM images in Fig. 5d that an inverse replica of the former woodpile structure has been obtained with the presented method. At higher magnifications (Fig. 8c and d) it becomes obvious that even after calcination the replicated titania still contains mesopores, which are present in an ordered fashion even in the tip of the shown structure (Fig. 8d). Figure 8c represents a nice example for the employed strategy as the two types of pores (macro- and mesopores) of the envisaged hierarchical pore structure are both visible.

Conclusion

The results presented here for producing hierarchically ordered pore structures show that it is possible to combine the laser-based top-down approach of structuring materials on the micrometer scale by 2PP with a chemical bottom-up self-organization process. Furthermore, we have demonstrated that the developed strategy is not limited to amorphous materials, as after calcination the amorphous titania has been transformed into crystalline anatase. Noteworthy, the refractive index of anatase of 2.6 and is

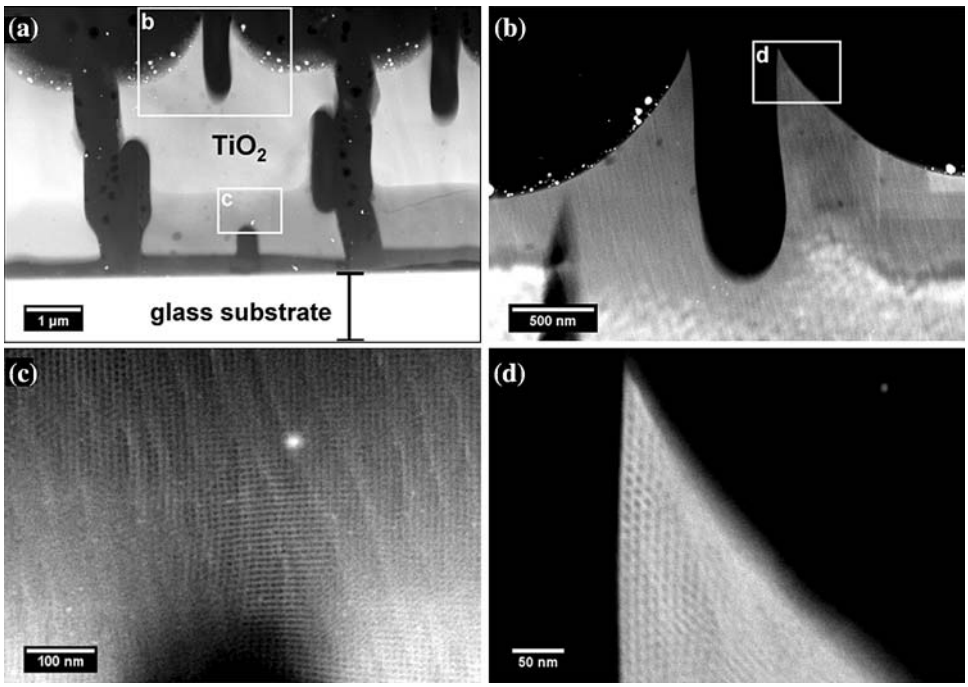

Fig. 8 Cross-sectional STEM images of a calcined titania structure at different magnifications. Differences in brightness of the titania structure visible in (**a**) can be ascribed to a preparation effect rather than to a distinct structural property

thus large enough for applications in photonics whereas for mixed silica–titania-based replicas prepared via a similar approach, this value is considerably lower, namely only 2.2. [31]. This phase transition is, however, accompanied by a drastically volume shrinkage which is responsible for a loss of structural precision in the woodpile structure. This could hamper applications in optical technologies. Inhibition or better control of the shrinkage process will thus be a challenging target for future investigations. However, for the meso-/macroporous structures presented here, either in their amorphous form after the post-synthetic treatment or in their crystalline from after calcination, possible applications in sorption and catalysis, but also as biomaterials in tissue engineering, can be envisaged.

References

1. Ostendorf A, Chichkov BN (2006) Photonics Spectra 40:72
2. Maruo S, Nakamura O, Kawata S (1997) Opt Lett 22:132
3. Kawata S, Sun H, Tanaka T, Takada K (2001) Nature 412:697
4. Cumpston BH, Ananthavel SP, Barlow S, Dyer DL, Ehrlich JE, Erskine LL, Heikal AA, Kuebler SM, Lee I-YS, McCord-Maughon D, Qin J, Röckel H, Rumi M, Wu X-L, Marder SR, Perry JW (1999) Nature 398:51
5. Serbin J, Egbert A, Ostendorf A, Chichkov BN, Houbertz R, Domann G, Schulz J, Cronauer C, Fröhlich L, Popall M (2003) Opt Lett 28:301
6. Deubel M, von Freymann G, Wegener M, Pereira S, Busch K, Soukoulis CM (2004) Nat Mater 3:444
7. Wong S, Deubel M, Pérez-Willard F, John S, Ozin GA, Wegener M, von Freymann G (2006) Adv Mater 18:265
8. Tétreault N, von Freymann G, Deubel M, Hermatschweiler M, Pérez-Willard F, John S, Wegener M, Ozin GA (2006) Adv Mater 18:457
9. Narayan RJ, Jin C, Doraiswamy A, Mihailescu IN, Jelinek M, Ovsianikov A, Chichkov BN, Chrisey DB (2005) Adv Eng Mater 7:108
10. Serbin J, Ovsianikov A, Chichkov BN (2004) Opt Express 12:5221
11. Kresge C, Leonowicz M, Roth W, Vartuli J, Beck J (1992) Nature 359:710
12. Beck J, Vartuli J, Roth W, Leonowitz M, Kresge C, Schmitt K, Chu C, Olson D, Sheppard E, McCullen S, Higgins J, Schlenker J (1992) J Am Chem Soc 114:10834
13. Yamada T, Zhou H, Uchida H, Honma I, Katsube T (2004) J Phys Chem B 108:13341
14. Maschmeyer T, Rey F, Sankar G, Thomas JM (1995) Nature 378:159
15. Yang P, Zhao D, Margolese DI, Chmelka B, Stucky G (1998) Nature 396:152
16. Braun PV, Osenar P, Stupp SI (1996) Nature 380:325
17. Zhao D, Luan Z, Kevan L (1997) Chem Commun 1009
18. Tian B, Liu X, Tu B, Yu C, Fan J, Wang L, Xie S, Stucky G, Zhao D (2003) Nat Mater 2:159
19. Zhao D, Yang P, Melosh N, Feng J, Chmelka B, Stucky G (1998) Adv Mater 10:1380
20. Grosso D, De AA, Soler-Ikkia G, Babonneau F, Sanchez C, Albouy P, Brunet-Bruneau A, Balkenende AR (2001) Adv Mater 13:1085
21. Brinker CJ, Lu Y, Sellinger A, Fan H (1999) Adv Mater 11:579
22. Grosso D, Cagnol F, De AA, Soler-Illia G, Crepaldi EL, Amenitsch H, Brunet-Bruneau A, Bourgeois A, Sanchez C (2004) Adv Funct Mater 14:309
23. Wirnsberger G, Yang P, Scott BJ, Chmelka BF, Stucky GD (2001) Spectrochim Acta A 57:2049
24. Turck C, Brandes G, Krueger I, Behrens P, Mojallal H, Lenarz T, Stieve M (2007) Acta Otolaryngol 127:801
25. Heinroth F, Bremer I, Münzer S, Behrens P, Reinhardt C, Pasinger S, Ohrt C, Chichkov BN (2009) Microporous Mesoporous Mater 119:104

26. Hermatschweiler M, Ledermann A, Ozin GA, Wegener M, von Freymann G (2007) Adv Funct Mater 17:2273
27. García-Santamaría F, Xu M, Lousse V, Fan S, Braun PV, Lewis JA (2007) Adv Mater 19:1567
28. Grosso D, De AA, Soler-Ikkia G, Crepaldi EL, Cagnol F, Sinturel C, Bourgeois A, Brunet-Bruneau A, Amenitsch H, Albouy PA, Sanchez C (2003) Chem Mater 15:4662
29. Chen W, Geng Y, Sun X, Cai Q, Li H, Weng D (2008) Microporous Mesoporous Mater 111:219
30. Henrist C, Dewalque J, Mathis F, Cloots R (2009) Microporous Mesoporous Mater 117:292
31. Baohua J, Shuhui W, Jiafang L, Min G (2007) J Appl Phys 102:96102
32. Passinger S, Saifullah MS, Reinhardt C, Subramanian KR, Chichkov BN, Welland ME (2007) Adv Mater 19:1218
33. Natl Bur Stand (U.S.) Monogr (1969) 25:82; JCPDS database no. 21-1272